Supplementary Information

for

Adsorption-driven Reverse Osmosis Separation of Ethanol/Water Using Zeolite Nanosheets

Yen-Yung Wu [a], Li-Chiang Lin *[ab]

[a]*Department of Chemical Engineering, National Taiwan University, No. 1, Sec. 4, Roosevelt Road, Taipei 10617, Taiwan.*

[b]*William G. Lowrie Department of Chemical and Biomolecular Engineering, The Ohio State University, 151 W. Woodruff Avenue, Columbus, Ohio 43210, USA.*

Li-Chiang Lin *E-mail: lclin@ntu.edu.tw

Table of Contents

1. Computational Details

1.1 Molecular Dynamics (MD) Simulations

Molecular dynamics (MD) simulations, implemented in the open-source LAMMPS package[1], are employed to investigate the separation performance of zeolite nanosheets as the RO membranes for the separation of ethanol and water. While some key details have been discussed in the main text, more information regarding these simulations is offered herein. In these calculations, both non-bonded and bonded potentials are used to describe the intermolecular and intramolecular interactions of nanosheet structures and each mixture component, as well as their interactions in between. The 12-6 Lennard-Jones (L-J) potential and the Coulombic potential with static point charges are employed to describe non-bonded interactions. The L-J potential is truncated and shifted to zero at a cutoff distance of 12 Å, while the long-range Coulombic interactions are computed using the particle-particle particle-mesh (PPPM) method with an accuracy of 10^{-6}. The geometric mixing rule is applied to calculate the parameters between different atom types. For bonded interactions, a harmonic model is used to describe bonds and angles, with OPLS-style dihedrals implemented for torsion contributions. A scaling factor of 0.5 is applied to account for 1-4 van der Waals intramolecular interactions. The non-surface regions of nanosheets, pistons, and water molecules are treated as rigid, while the surface regions (i.e., Si-OH) of nanosheets are considered flexible. The L-J parameters for the carbon atoms of the two rigid graphene pistons are adapted from the OPLS-AA force field[2]. For each equilibrium MD (EMD) simulation, an initial equilibration run of at least 10 ns is performed to saturate the membrane until the density of ethanol and water inside and that on the surface of the nanosheet

membrane remains unchanged. Subsequently, the feed solution is replenished by adding additional ethanol molecules to match the targeted feed condition (i.e., 40 wt.%). Non-equilibrium MD (NEMD) runs of at least 20 ns are then carried out to quantify the membrane's separation performance (i.e., separation factor and thickness-normalized flux).

1.2 Integrated Approach Utilizing Isobaric-isothermal and Gibbs Ensemble Monte Carlo Simulations and Grand Canonical Monte Carlo Calculations

The isobaric-isothermal and Gibbs ensemble Monte Carlo[3, 4] (NPT-GEMC) simulations, followed by grand canonical Monte Carlo (GCMC) calculations[5], are conducted using the open-source RASPA[6] software to determine the adsorption selectivity of bulk zeolite structures. Traditional NPT-GEMC simulation setups typically involve two separate boxes: one containing the liquid ethanol/water mixture at a specified concentration and another representing the zeolite structure of interest. However, direct swaps of species between these two dense phases result in very low acceptance probabilities[3, 4]. To address this issue, we adopt a two-step approach. In the first step, NPT-GEMC simulations are performed with also two domains but they are the liquid mixture and a constant-volume vapor phase. The objective of this step is to obtain the pressure and composition of the equilibrium vapor phase of the liquid mixture. The fugacity coefficient of the two components can then be subsequently determined using the Peng-Robinson equation of state[7] (PR-EOS). We note that, prior to the NPT-GEMC simulations, the liquid mixture box undergoes pre-equilibration using a NPT ensemble, consisting of 50,000 initialization cycles and 250,000 production cycles. In the second step, with the equilibrium vapor-phase fugacity and composition determined from the NPT-GEMC simulations, GCMC simulations are further conducted to calculate the adsorption selectivity of ethanol over water in bulk zeolites. Each GCMC simulation consists of 50,000 cycles for equilibration, followed by an additional 500,000 cycles to obtain statistical ensemble averages. The same force field used in the MD

simulations is employed in these calculations, except that ethanol molecules are treated as rigid for simplicity.

1.3 Osmotic Pressure of Ethanol/Water Mixture

In RO processes, a sufficiently large transmembrane pressure must be applied to overcome the osmotic pressure difference. To this end, we have also determined the osmotic pressure difference between a 40 wt.% ethanol/water mixture and a pure ethanol solution. The FER nanosheet membrane that is found to be nearly semi-permeable to ethanol is used in these calculations. Specifically, NEMD simulations are conducted under five different applied pressures (i.e., 25, 50, 100, 150, and 200 MPa), and three individual runs are carried out for each pressure for more accurate statistics. **Fig. S1** shows the total flux as a function of applied pressure. The total flux is observed to increase linearly, as would be expected, with the applied pressure, and an osmotic pressure difference of approximately 29.46 MPa is found. Aside from the direct computation, the osmotic pressure difference can also be theoretically calculated by eqn S1:

$$\Delta\pi = -\frac{RT}{V_{m,H_2O}} ln\left(\gamma_{H_2O} x_{H_2O}\right) \quad (S1)$$

where R is the universal gas constant, T, V_m, γ, and x are the absolute temperature (K), molar volume (m^3/mol), activity coefficient, and mole fraction, respectively. In eqn S1, V_m is determined based on a prior study of Delgado et al.[8], and γ is calculated by non-random two-liquid (NRTL) thermodynamic model[9] using Aspen plus V10. Provided that the membrane is semi-permeable to ethanol, the calculation herein considers ethanol as the solvent while having water act as the solute. **Fig. S2** shows the activity coefficient of water and ethanol at a pressure of 0.1 MPa. With the activity coefficient at x_{EtOH} = 0.2 (corresponding to 40 wt.%), the resulting osmotic pressure difference is

approximately 21.38 MPa, which aligns quite closely with the values determined by direct NEMD calculations.

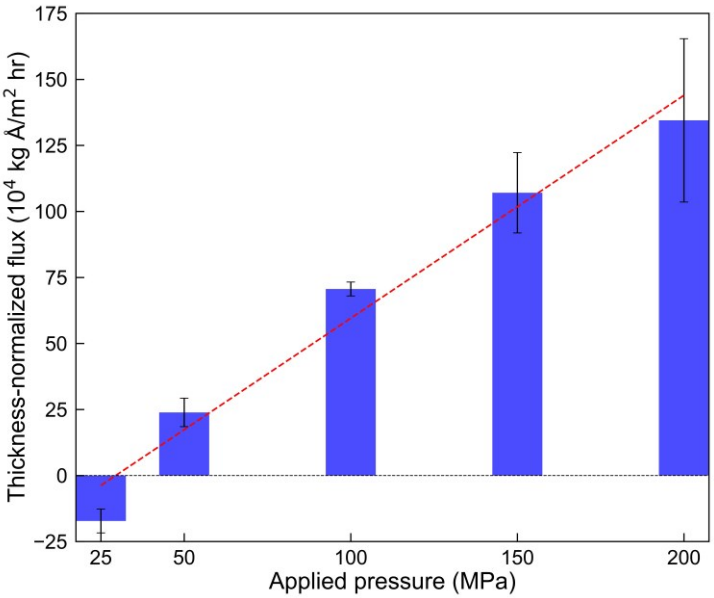

Fig. S1 NEMD-computed total flux as a function of applied pressure, using the zeolite FER nanosheet structure as the active layer.

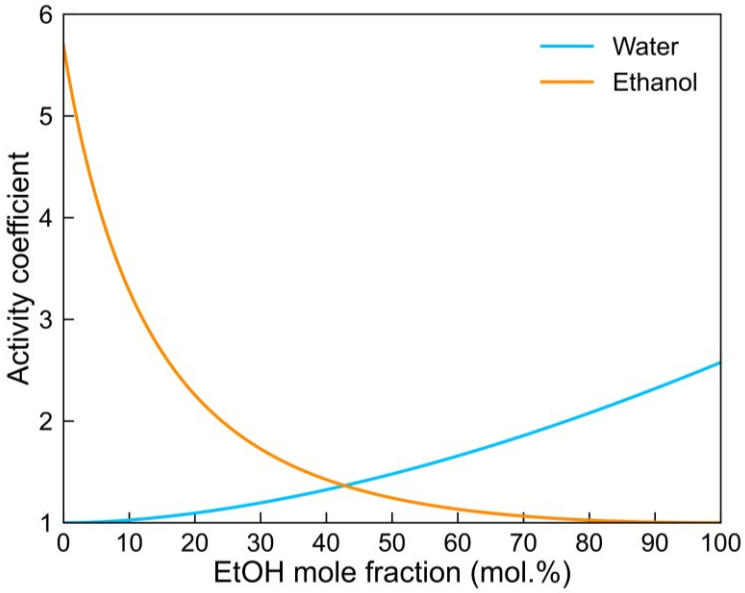

Fig. S2 Activity coefficient as a function of ethanol mole fraction for ethanol/water mixtures at a pressure of 0.1 MPa using the NRTL model.

1.4 Calculations of the Surface and Entrance Ethanol Mole Fraction

The surface region of each nanosheet is defined to have a total thickness of 5 Å, extending from 1 Å inward from the outermost Si atom and 4 Å outward (see **Fig. S4**). The entrance region is characterized as a cylinder with the same thickness with a diameter equal to the channel opening. To determine the surface and entrance ethanol concentrations for each studied nanosheet, a total of 200 configurations collected from NEMD simulations are analyzed. For each configuration, the quantities of carbon (i.e., ethanol) and oxygen (i.e., water) within the defined surface layer or the entrance region are counted to compute the corresponding ethanol concentration.

1.5 Self-Diffusivity of Ethanol/Water Mixture in Nanosheet Membranes

MD simulations are carried out to probe the self-diffusivity of ethanol and water in the bulk structure of zeolites (i.e., in periodic 3D structures). Specifically, the loading values of ethanol and water in these calculations are per the steady-state condition of the bulk-phase observed in NEMD RO simulations with a double membrane thickness. **Table S1** shows the number of ethanol and water molecules per unit cell for each zeolite structure. In these calculations, canonical Monte Carlo simulations are first conducted to pre-equilibrate the system to a thermodynamically favorable state, followed by 50 ns MD calculations, also in a canonical ensemble, to collect molecular trajectories for subsequent analyses. All the force field and simulation parameters are consistent with the above-mentioned calculations. The self-diffusion coefficients of each adsorbate are determined by analyzing their mean squared displacement (MSD) as a function of time using the Einstein equation with the order-n algorithm[10]. The diffusion selectivity can then be calculated by the diffusivity ratio of ethanol over water. We note that amongst the studied 14 structures, the self-diffusivity of water in some structures cannot be computed. Specifically, the diffusive region of water in MFI-zigzag and MTT cannot be reached within an already long MD time of 50 ns. For MRE, given no water molecules are observed in the bulk-phase region during the RO simulations, it's water diffusivity cannot be determined. Although the diffusion selectivity cannot be determined for all studied structures, as discussed in the main text, the results have evidently suggested that the diffusion selectivity does not play a key role in controlling the observed RO separation performance.

Table S1 The number of ethanol and water within the bulk-phase region of each nanosheet structure.

The numbers in the block denote the amount that exists within the unit-cell structures.

Structure	Number of EtOH	Number of H_2O	Structure	Number of EtOH	Number of H_2O
FER	3.25	0.083	BEC_a	2.94	0.50
FER_r	3.04	0.083	BEC_c	5.39	2.33
MFI	7.42	0.17	ATS	4.03	0.33
MFI-zigzag	17.25	0.17	IWV	43.88	9.75
MTT	2.1	0.10	AET	8.22	2.00
MRE	3.17	0	ETR	20.00	18.33
OSI	2.4	0.75	IRR	155	315

2. Additional Figures and Tables Referred in the Main Text

Table S2 Kendall's tau (upper triangular cells in white) and Pearson (lower triangular cells in grey) correlation coefficients at a significance level of 0.05.

Kendall's tau / *Pearson*	*Flux*	*Separation factor*	*PLD*	*LCD*	*Adsorption selectivity*	*Bulk solubility*	*Surface fraction*	*Entrance fraction*	*Permeate concentration*
Flux	1.00	-0.23	0.45	0.47	-0.65	-0.32	-0.14	-0.21	-0.19
Separation factor	-0.22	1.00	-0.67	-0.65	0.51	0.74	0.03	0.19	0.91
PLD	0.83	-0.49	1.00	0.84	-0.61	-0.58	-0.04	-0.18	-0.69
LCD	0.90	-0.44	0.97	1.00	-0.68	-0.60	0.02	-0.16	-0.67
Adsorption selectivity	-0.25	0.75	-0.35	-0.35	1.00	0.69	0.07	0.16	0.45
Bulk solubility	-0.14	0.69	-0.19	-0.21	0.98	1.00	0.16	0.23	0.65
Surface fraction	-0.01	0.29	0.15	0.19	0.15	0.19	1.00	0.41	0.03
Entrance fraction	-0.14	0.46	-0.08	-0.11	0.27	0.29	0.60	1.00	0.19
Permeate concentration	-0.35	0.54	-0.67	-0.57	0.36	0.28	-0.18	-0.20	1.00

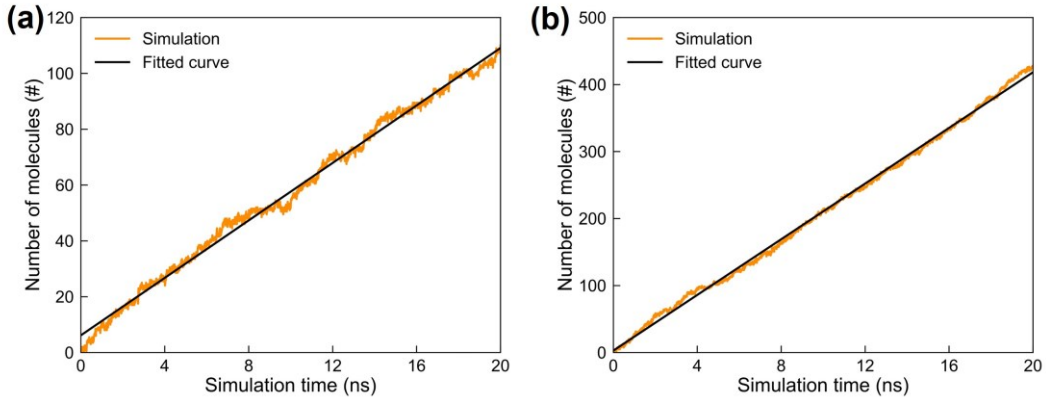

Fig. S3 The number of permeated ethanol observed in the permeate-side region as a function of simulation time using (a) a smaller domain size (i.e., 4-fold smaller than the simulation domain in this work) and (b) the size used to compute all the reported results in the main text, with their corresponding linear regression line presented in black. Simulations using an enlarged domain can evidently observe more stable flow with notably smaller fluctuations.

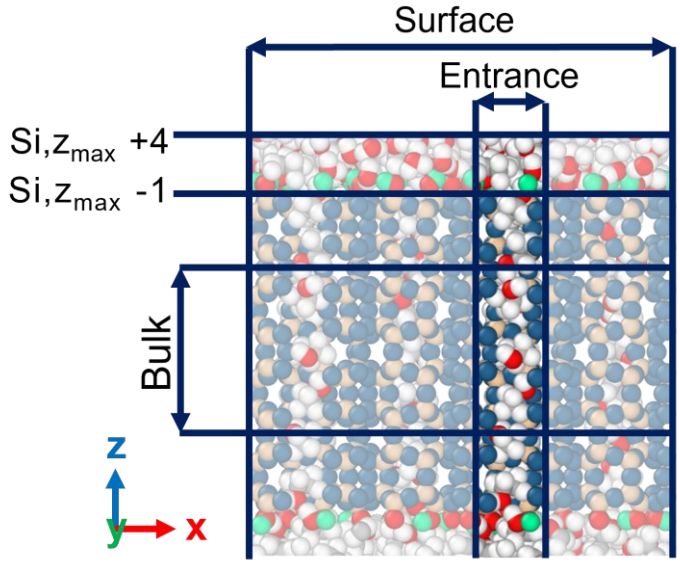

Fig. S4 Schematic illustrations of surface and bulk regions of the simulation domain. The surface region is characterized by a total thickness of 5 Angstroms. The layer spans 1 Å inward from the outermost Si atom and 4 Å outward from it, as shown in the figure. The entrance section refers to the portion of the surface region that is located near the channel opening along the permeation direction (i.e., z-direction). The bulk region is defined as the center portion of the zeolite (i.e., along the z-direction) with a dimension that is a half of the distance between the two outermost Si atoms. This region is anticipated to be less affected by the external surface of the membrane and is used to determine the solubility selectivity.

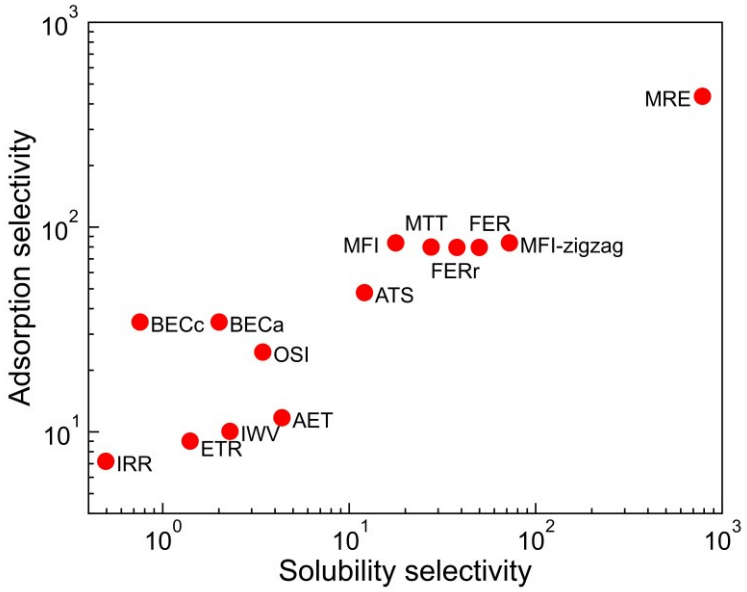

Fig. S5 Bulk-phase solubility selectivity determined per NEMD trajectories versus adsorption selectivity computed by the approach utilizing NPT-Gibbs coupled with GCMC. Their Kendall's tau correlation coefficient is computed to be 0.69.

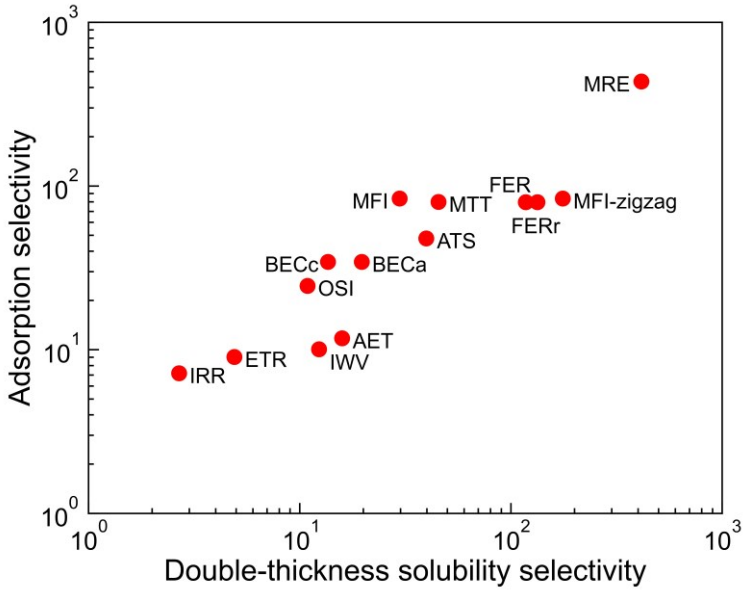

Fig. S6 The solubility selectivity determined per NEMD trajectories with a double membrane thickness versus the Monte Carlo-computed adsorption selectivity. Their Kendall's tau correlation coefficient is computed to be 0.78.

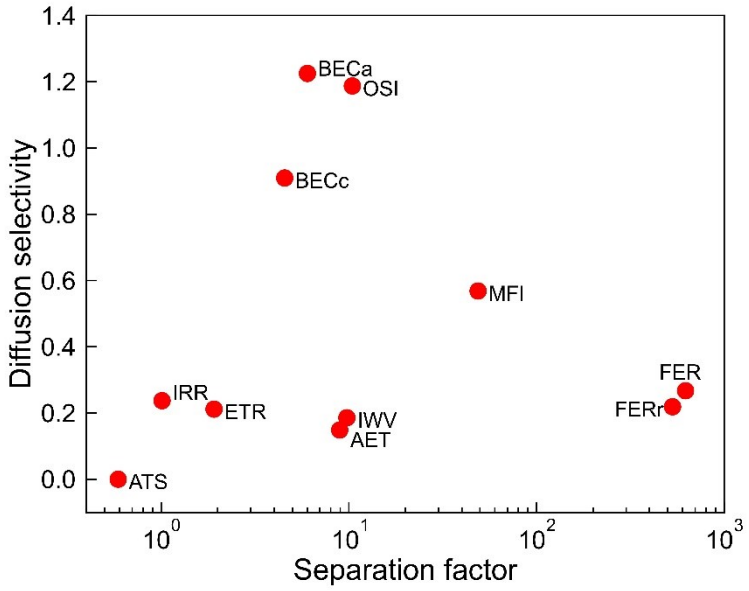

Fig. S7 Correlation between the ethanol-to-water diffusion selectivity and the RO separation factor. The self-diffusivity is calculated under the steady-state condition of the bulk-phase in each nanosheet candidate observed in NEMD RO simulations with computational details shown in the ESI. It should be noted that, although the diffusive region appears to be achieved with a slope of ln(MSD) vs. ln(Δt) to be approximately one for zeolite ATS that has a very restricted diffusivity, its diffusion region is chosen to be the very last few sampling points. The Kendall's tau coefficient between the diffusion selectivity and the separation factor is 0.20.

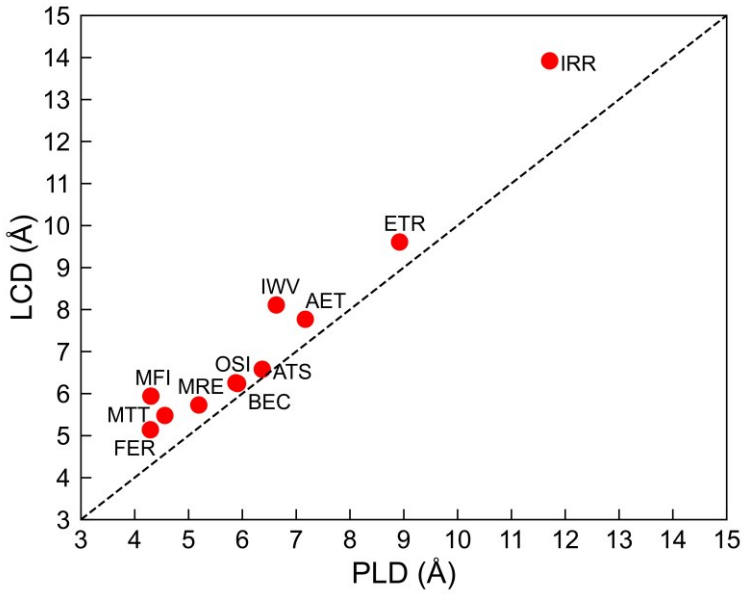

Fig. S8 The similarity between the PLD and LCD of studied zeolites.

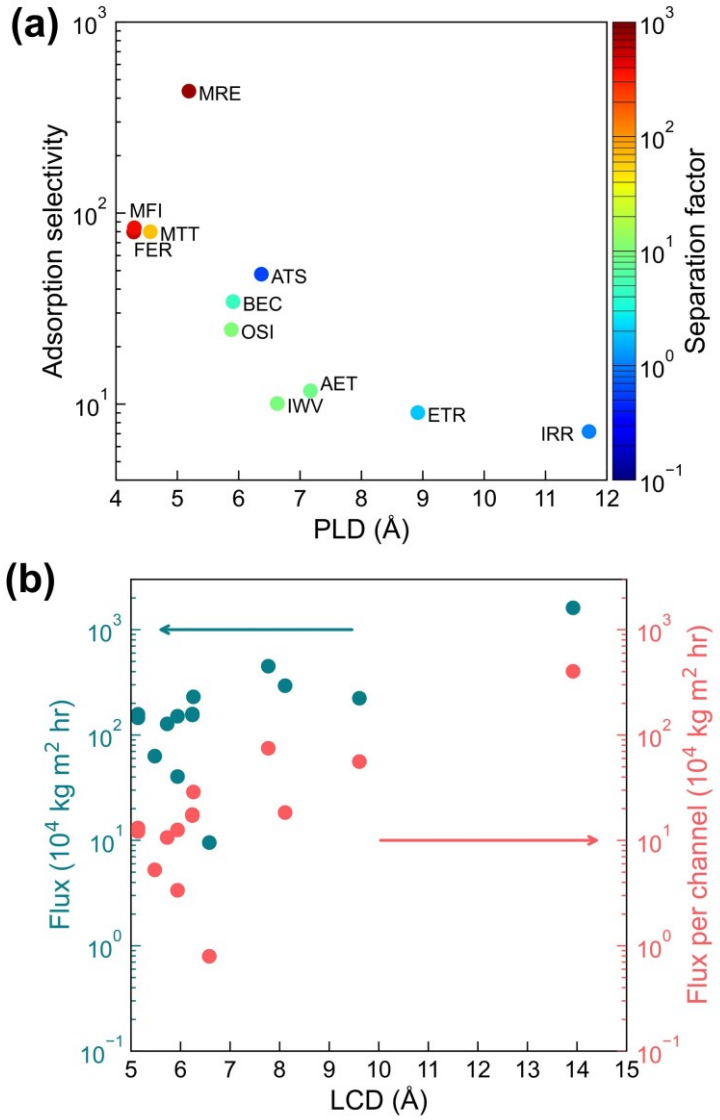

Fig. S9 (a) Correlation between the adsorption selectivity and PLD, with each data point color-coded according on separation factor. The separation factor values shown for MFI, FER and BEC are that of MFI-zigzag, FER and BEC_a, respectively. (b) Correlation between the thickness-normalized flux (left axis) and the normalized flux per channel (right axis) with LCD.

3. References

1. S. Plimpton, *J. Comput. Phys.*, 1995, **117**, 1-19.
2. W. L. Jorgensen, D. S. Maxwell and J. Tirado-Rives, *J. Am. Chem. Soc.*, 1996, **118**, 11225-11236.
3. A. Z. Panagiotopoulos, N. Quirke, M. Stapleton and D. J. Tildesley, *Mol. Phys.*, 1988, **63**, 527-545.
4. A. Z. Panagiotopoulos, *Mol. Phys.*, 1987, **61**, 813-826.
5. B. Smit, *Mol. Phys.*, 1995, **85**, 153-172.
6. D. Dubbeldam, S. Calero, D. E. Ellis and R. Q. Snurr, *Mol. Simul.*, 2016, **42**, 81-101.
7. D.-Y. Peng and D. B. Robinson, *Ind. Eng. Chem. Fundam.*, 1976, **15**, 59-64.
8. D. R. Delgado, M. Á. Peña and F. Martínez, *Rev. Colomb. Cienc. Quim.-Farm.*, 2013, **42**, 298-314.
9. H. Renon and J. M. Prausnitz, *AlChE J.*, 1968, **14**, 135-144.
10. D. Dubbeldam, D. C. Ford, D. E. Ellis and R. Q. Snurr, *Mol. Simul.*, 2009, **35**, 1084-1097.